DYNAMIC SURFACE PRESSURE MEASUREMENTS ON A FLAPPING WING IN SMOOTH AND TURBULENT FLOW

Alex Fisher, Simon Watkins, and Jon Watmuff
RMIT University, Melbourne, Australia
alex.fisher@rmit.edu.au, simon@rmit.edu.au, jon.watmuff@rmit.edu.au

Abstract

Time-resolved measurements of surface pressure at various spanwise positions on a thin wing in simple root-flapping motion are presented. Pressure distributions during the downstroke exhibit a large suction peak which eventually broadens and moves downstream. Smoke flow visualization confirms this to be caused by a leading-edge vortex (LEV). Measurements are conducted in nominally smooth flow, as well as two grid-generated turbulence conditions designed to replicate atmospheric turbulence as best as possible. Results of tests in turbulence reveal a narrowing of the hysteresis loop at low reduced frequency, and a broadening of the LEV suction peak when present. The effect of turbulence appears to diminish as reduced frequency is increased.

1 Introduction

There has been much interest in the aerodynamics of flapping wings of late, mainly due to their possible application in micro air vehicles (MAVs). While there is no single definition of an MAV, wing spans of less than 1 meter and maximum speeds of less than 10 m/s are typical. Thus MAVs operate at a low Reynolds number (< 100,000), where performance of fixed wings drops significantly [7]. Early studies applying quasi-steady analysis to insect wings did not explain the high lift insects are able to generate in order to support their weight [13]. Since then numerous mechanisms have been proposed by which insects could generate extra lift. One such mechanism is “clap-and-fling” [13], by which the insect avoids the negative influence of starting vortices by clapping the wings together at the start of a stroke. Another is “rotational circulation”, wherein a lift increment is achieved by quickly rotating the wings at the end of each stroke [2]. Interaction of the flapping wing with the wake left behind by previous strokes can also lead to a lift increase, although this principally applies to hovering [3, 14].

Arguably the most important of the unsteady mechanisms is the leading edge vortex (LEV). The LEV is a concentrated area of vorticity above the wing which can induce strong suction on the upper surface, thereby increasing lift. The LEV is created by self-induced rollup of the shear layer shed from the leading edge during leading edge separation [9]. In this way the LEV is similar to a laminar separation bubble (LSB); however LSBs require transition to turbulence to induce reattachment, whereas attached LEVs can be found in entirely laminar flow (e.g. insect flight at Re O(100)) [5]. The LEV plays an important role in the dynamic stall behaviour of traditional airfoils, however the increase in lift it induces is usually only sustained momentarily. As long as the flow is separated at the leading edge, the LEV is fed with more vorticity, thus it grows in size until it can no longer remain attached, and is eventually shed and advected downstream. In studies of 2D airfoils, the LEV is found to detach after a certain time; thus it has been theorized that to obtain maximum benefit from the LEV, a flapping wing should match the time it takes to perform one stroke, with the time it takes for the LEV to be shed [11]. However, the investigation of 3D wings has revealed that LEVs can remain attached for much longer than they do in 2D,

perhaps even indefinitely for wings in continuous rotation [10]. The mechanism by which the LEV can remain attached in a 3D flapping wing is still not fully understood, but a recent study has suggested it is facilitated by centrifugal and Coriolis forces [5]. The effect of Reynolds number on LEV behavior is also poorly understood.

An aspect of MAV flight often overlooked is the presence of high levels of turbulence in the typical operational environment. MAV operation is typically confined to the lower portion of the atmospheric boundary layer (ABL) which often exhibits turbulence due in part to thermal/shear layer instability, but also local disturbances introduced by wind flow over obstacles such as buildings and trees. On windy days turbulence intensities up to 30% are not uncommon [6]. While the integral scales of atmospheric turbulence are large with respect to the size of a typical MAV, there is still significant energy present at the smaller scales [12], which has been shown to affect the aerodynamics of fixed wing MAVs in a manner that is not able to be predicted by quasi-steady analysis [8]. The aim of the current study is to explore the effect of replicated atmospheric turbulence on a wing in unsteady motion typical of a potential flapping-wing MAV.

2 Experimental Setup

2.1 Flapping Rig

The flapping rig consisted of a single wing of (semi) aspect ratio 2, and a large (1.5m × 1.5m) reflection plane (Fig. 1). In its neutral position the wing was vertical. The flapping motion was achieved by means of a stepper motor, situated approximately 4 chord lengths downstream of the wing, which was connected to the wing via a steel shaft running through a channel cut into the reflection plane. The motor was driven by a 70VDC stepper motor driver (GeckoDrive G203V), connected to a microcontroller (Microchip dsPIC30F4011), which was in turn connected to a PC.

Custom software and microcontroller firmware were written to provide step signals to the driver and to provide a synchronization signal in order to synchronize the pressure measurements to the flapping motion. The motion was a ±45° sine wave for all tests. Although driving the stepper motor open-loop is reliable, the motion was always verified by means of a precision potentiometer attached to the main shaft. The deterministic nature of the control system meant that the motion was very consistent cycle-to-cycle; the maximum standard deviation of wing position (across any given run of 200 flapping cycles), at any point in the cycle as measured by the potentiometer was 0.08°, a significant portion of which may have been due to potentiometer backlash which was stated by the manufacturer as ±0.1°.

Fig. 1. Flapping model.

2.2 Wings

Four wings were constructed, all identical except for the fact that each had a chordwise row of pressure taps at a different spanwise location. The locations were 38%, 58%, 69%, and 85% of the semi-span (measured from the root). Each wing had 17 taps on the upper surface, 16 on the lower, and one at the leading edge.

The main wing box structure was made from carbon fiber, while the leading and trailing edges were made by Objet stereolithography (Fig. 2). Pressure taps were connected to 1mm

inner diameter PVC tubes, which ran inside the wing and exited at the root. The tubes were then connected to stationary transducer banks below the reflection plane. The length of tubing combined with the fact that the tubes inside the wing were being accelerated during flapping meant that the pressure signal appearing at the transducers was significantly distorted. This distortion was corrected for, and a detailed calibration exercise was performed in order to ensure that this correction was accurate.

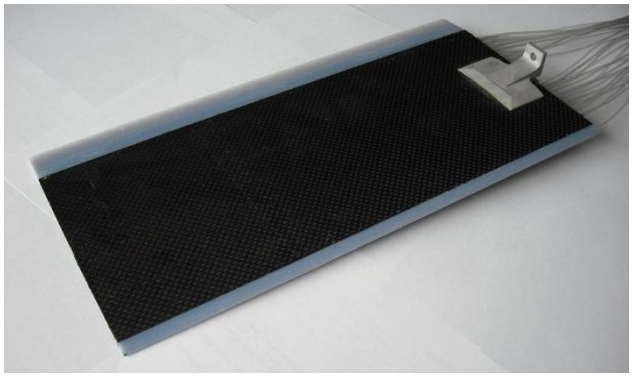

Fig. 2. Pressure-tapped wing.

2.2 Pressure Measurement System

The Dynamic Pressure Measurement System (DPMS) provided by Turbulent Flow Instrumentation, Inc. (TFI) was used to obtain pressure measurements. It consisted of 4 banks of 15 pressure transducers together with a multiplexer to allow connection to a 16 channel DAQ card inside a PC. The transducers had a frequency response up to 1kHz.

The length of tubing connecting the taps to the transducers was around 550mm. This causes the pressure fluctuations to be distorted as they travel through the tube due to a combination of the organ pipe resonance effect and viscous damping. Fortunately at the amplitudes involved such distortion is linear and as such can be corrected if the transfer function is known. The correction involved applying the inverse of the transfer function to recover the pressure time history at the tap, done efficiently in the digital domain by means of the overlap-save method.

An accurate theoretical model to predict the transfer function is available, however such a model cannot account for slight differences in the manufacturing of tubes, differences in transducer response, etc. To ensure best possible accuracy, each tap on each wing was individually calibrated by applying a known waveform consisting of a mix of frequencies from 10 to 100Hz (the range of interest) and measuring the result to obtain the transfer function. Data from each tap was then corrected using its own unique transfer function during post-processing. The result was a flat frequency response of the system up to 100Hz.

Another source of distortion was the fact that the tubes inside the wing were rotating. The resulting centrifugal force was strong enough to cause a significant pressure drop along the length of tube. Fortunately this effect also behaved linearly (as verified by laminar CFD simulations) and could thus be corrected for since the wing motion was known accurately.

Considering all sources of error, a conservative upper bound on measurement uncertainty for pressure coefficient is ±0.05; for integrated lift coefficient ±0.03.

2.3 Wind Tunnel and Grids

Tests were performed in the RMIT University Industrial Wind Tunnel with a working section measuring 2m × 3m × 9m. It was desirable to use as large a facility as possible, as the turbulence conditions under test were designed to replicate atmospheric conditions of large integral length scale. Tests were conducted under two different turbulence conditions, as well as in nominally smooth flow. The different turbulence conditions were generated by positioning a grid upstream of the contraction, and at the test section inlet. This resulted in turbulence intensities of 7% and 13% for the two conditions, with streamwise integral length scales of 0.15m and 0.31m respectively. Turbulence intensity for the nominally smooth flow condition was 1.2%. Turbulence properties

were measured using a four-hole "Cobra" probe supplied by TFI.

The presence of the large reflection plane had a noticeable effect on the turbulence characteristics in the vicinity of the wing. However this effect was principally on the spanwise velocity component; the vertical and streamwise components, considered to have the greatest effect on the resulting aerodynamic performance of the wing, were much less affected.

2.4 Smoke Wire System

The smoke wire system consisted of 0.08mm nichrome wire, a 60VDC power supply, a digital camera with external flash, and a microcontroller-based synchronization circuit. By coating the wire in glycerin and running a current through it, small filaments of smoke are produced. The wire was suspended between two vertical rods mounted into the reflection plane. The rods were positioned 30cm either side of the wing so that their influence on the flow was negligible. The wire was positioned 2cm in front of the leading edge; while this is relatively close, the diameter of the wire was sufficiently small as to not affect the flow significantly (this was verified by taking pressure measurements with the wire present).

At the velocity under test, the smoke filaments lasted approximately 1 second. In order to repeatably obtain images at specific phases of the flapping cycle, the timing of the camera, flash, and smoke wire current had to be precisely controlled relative to the flapping motion. The firmware in the controller circuit took input from the flapping rig's synchronization signal, and then calculated in real time at what point to activate the smoke wire, open the camera shutter, and fire the flash. Some fine-tuning was required to account for the delay in vaporizing the glycerin and opening the camera shutter, but consistent results were eventually achieved.

3 Results and Discussion

Tests were performed at reduced frequencies of 0.075, 0.15, 0.225, and 0.3. Angle of attack was set at 0, 4, 8, and 12°. Resulting phase-averaged "instantaneous lift coefficients" (i.e. lift non-dimensionalized using the instantaneous velocity at the spanwise position in question) are plotted against instantaneous section angle of attack (i.e. that taking into account the angle of attack induced by the flapping motion) for the k = 0.075 case in Figs 3, 4, and 5. For reference the static values at the appropriate spanwise position are also shown.

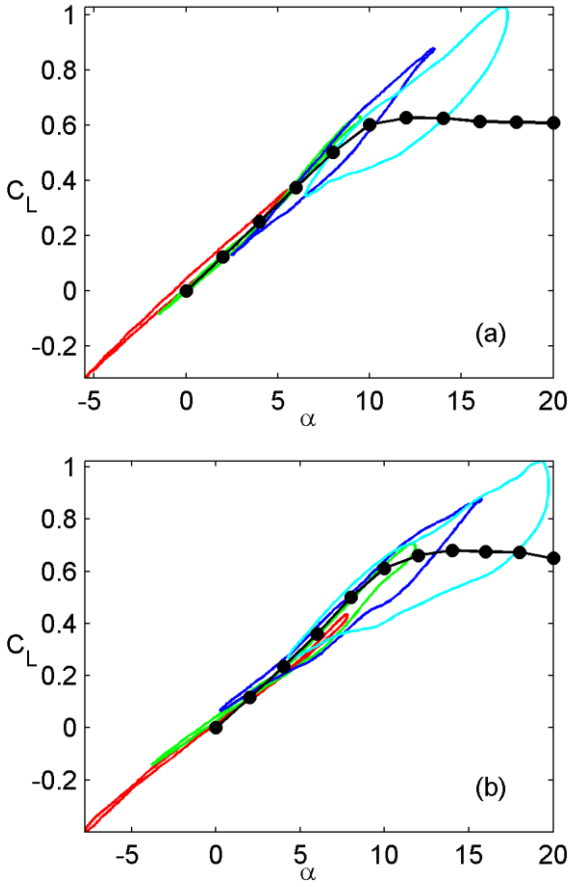

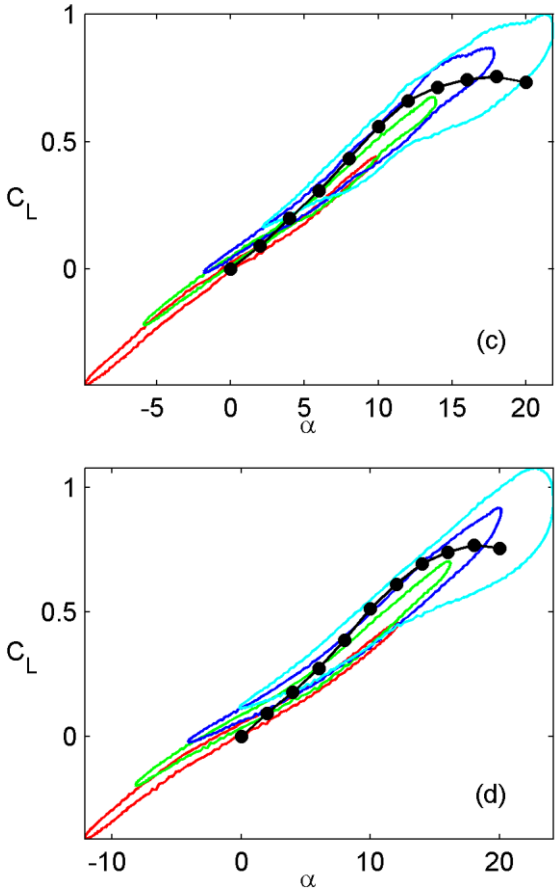

Fig. 3. Sectional lift curves in nominally smooth flow, k = 0.075, at (a) 38%, (b) 58%, (c) 69%, and (d) 85% semi-span.

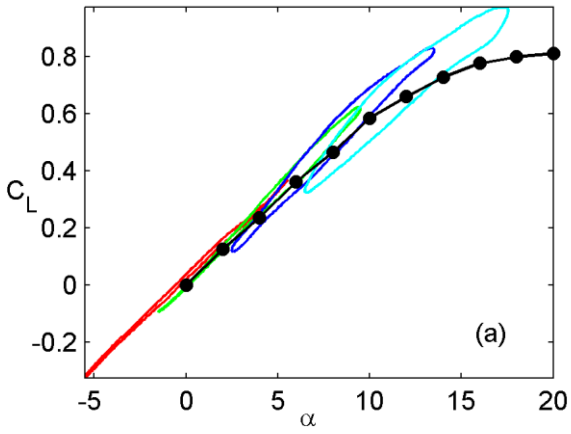

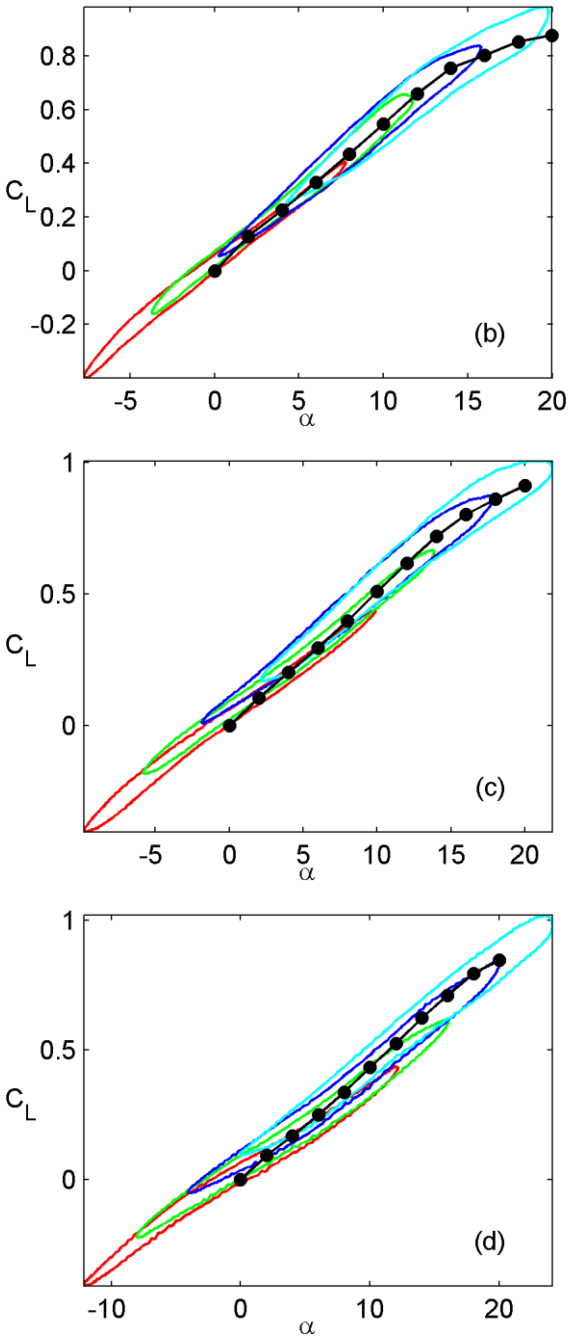

Fig. 4. Sectional lift curves in 7% turbulence intensity, k = 0.075, at (a) 38%, (b) 58%, (c) 69%, and (d) 85% semi-span.

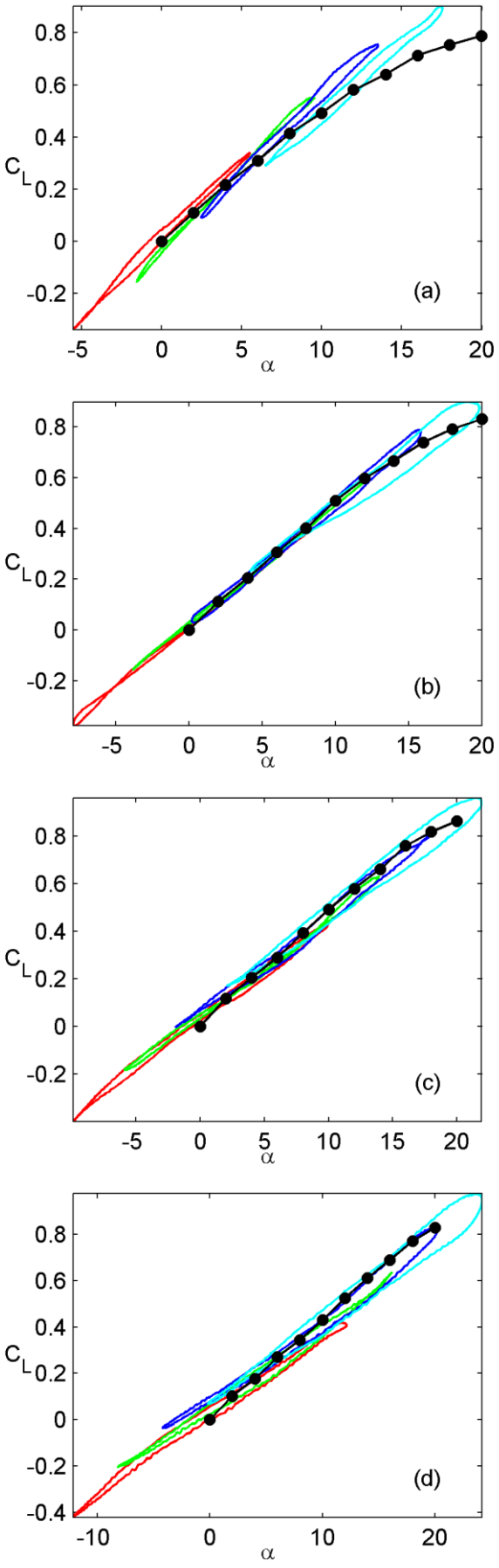

Fig. 5. Sectional lift curves in 13% turbulence intensity, k = 0.075, at (a) 38%, (b) 58%, (c) 69%, and (d) 85% semi-span.

Reasonable agreement with the static values and little hysteresis is observed when the instantaneous angle of attack remains in the linear region. Although perhaps within the experimental error, a slight increase in hysteresis as spanwise position moves towards the tip is noted in these cases. This is likely due to an increase in the added mass component of the net force, as greater linear acceleration is experienced toward the tip.

Despite the low reduced frequency, significant lift overshoot from the steady values together with a wide hysteresis loop is present when the angle of attack extends into the stalled region. In the return from stall lift is generally below static values, consistent with traditional dynamic stall [1] and other flapping wing experiments [4].

Noticeable across all results (but more marked when the angle of attack remains in the linear region) is a trend of decreasing lift curve slope relative to the static results as spanwise position moves towards the tip. The reason for this is not certain, but it may be a result of the relative tip vortex strength on the flapping wing as compared to the fixed.

The effect of turbulence is to produce a decrease in lift curve slope and a narrower hysteresis loop. The narrowing hysteresis loop is likely due to reattachment being aided by additional turbulent mixing on the return from stall.

The net effect of increased turbulence diminishes as *k* is increased (for example see Fig. 6). Here lift values for all cases remain similar (possibly even the same given the error bounds) for the majority of the flapping cycle, with the exception of a small region as the maximum angle of attack is approached. The pressure distributions (shown in Fig. 7 for k = 0.3) show that this is mainly caused by a flattening of the LEV suction peak. Fig. 7 also serves to illustrate the evolution of the LEV suction peak at mid semi-span; the

corresponding flow visualization images in Fig. 8 show the growth of the LEV.

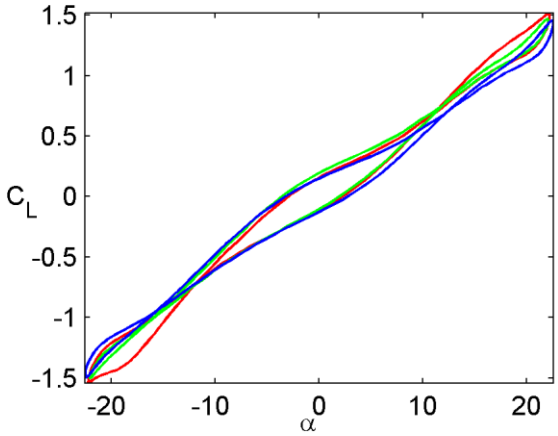

Fig. 6. Sectional lift curves at 58% semi-span for smooth flow (red), 7% turbulence intensity (green), and 13% turbulence intensity (blue); k = 0.225.

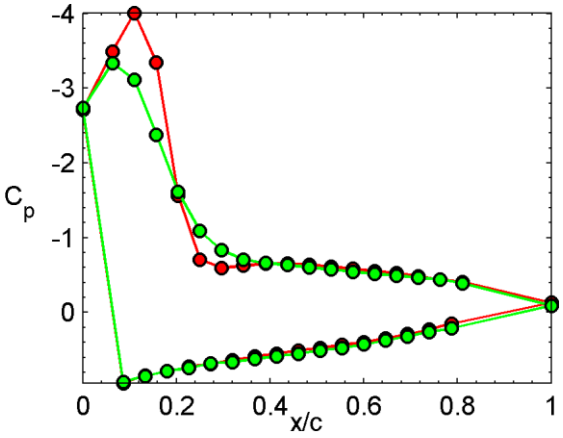

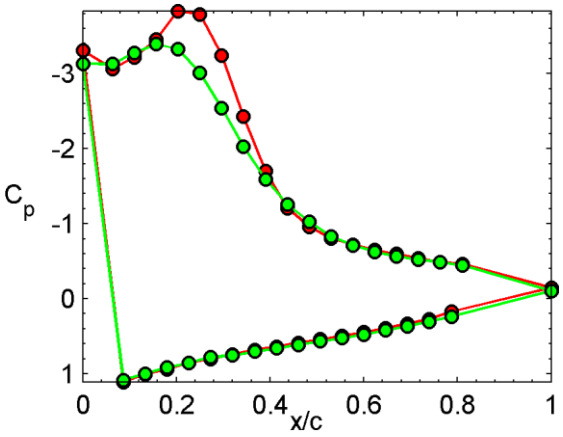

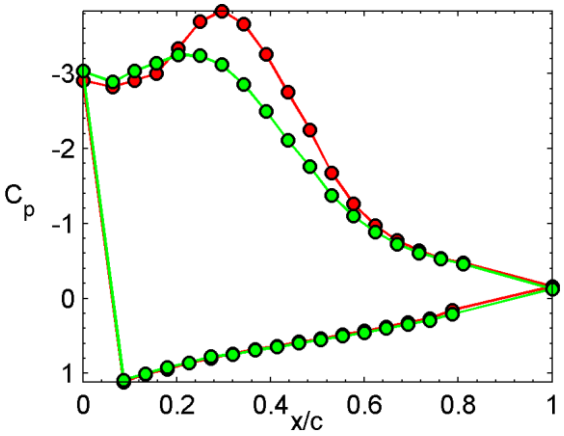

Fig. 7. Phase averaged pressure coefficient distributions; 58% semi-span, k = 0.3, smooth flow (red) and 13% turbulence intensity (green). t/T (a) 0.120, (b) 0.184, (c) 0.224.

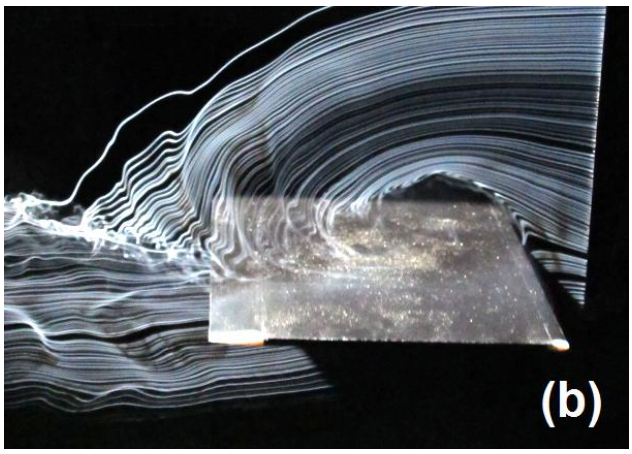

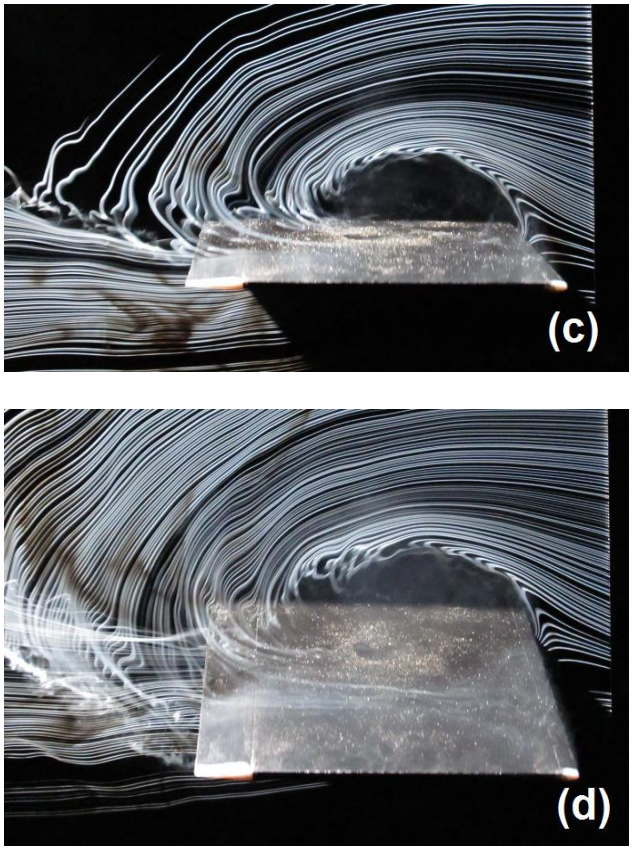

Fig. 8. Evolution of leading edge vortex; nominally smooth flow, $\alpha_{mean} = 0$, $k = 0.3$, smoke wire at 58% semi-span, t/T (a) 0.187, (b) 0.225, (c) 0.262, and (d) 0.300

4 Conclusions

The most significant result from data analysis conducted thus far appears to be that the net effect of turbulence significantly decreases as reduced frequency of a flapping wing is increased. This may be a first hint as to why flapping flight in turbulent conditions is so successful in nature.

Experiments are ongoing into the effect of turbulence on the wing undergoing other unsteady motions such as oscillations in pitch and combined pitching and flapping.

5 Acknowledgements

The authors would like to thank the USAF for funding aspects of this work via the AFOSR AOARD scheme, the Australian Federal Government for an APA scholarship and acknowledge the RMIT University technical staff for their help in constructing the flapping model.

References

[1] L W Carr, K W McAlister, and W J McCroskey. Analysis of the development of dynamic stall based on oscillating airfoil experiments. Technical report, NASA Ames Research Center, 1977.

[2] M H Dickinson. The effects of wing rotation on unsteady aerodynamic performance at low Reynolds numbers. *Journal of Experimental Biology*, 192:179–206, 1994.

[3] M H Dickinson. Wing rotation and the aerodynamic basis of insect flight. *Science*, 284:1954–1960, 1999.

[4] T Y Hubel and C Tropea. Experimental investigation of a flapping wing model. *Experiments in Fluids*, 46:945–961, 2009.

[5] D Lentink and M H Dickinson. Biofluiddynamic scaling of flapping, spinning and translating fins and wings. *Journal of Experimental Biology*, 212:2691–2704, 2009.

[6] J Milbank, B J Loxton, S Watkins, and W H Melbourne. Replication of atmospheric conditions for the purpose of testing mavs. RMIT, 2005.

[7] T J Mueller. *Fixed and Flapping Wing Aerodynamics for Micro Air Vehicle Applications*. American Institute of Aeronautics & Astronautics, 2002.

[8] S Ravi. *The Influence of Turbulence on a Flat Plate Airfoil at Reynolds Numbers Relevant to MAVs*. PhD thesis, RMIT University, 2011.

[9] S P Sane. The aerodynamics of insect flight. *Journal of Experimental Biology*, 206:4191–4208, 2003.

[10] J R Usherwood and C P Ellington. The aerodynamics of revolving wings i. model hawkmoth wings. *Journal of Experimental Biology*, 205:1547–1564, 2002.

[11] Z J Wang. Vortex shedding and frequency selection in flapping flight. *Journal of Fluid Mechanics*, 410:323–341, 2000.

[12] S Watkins, J Milbank, B J Loxton, and W H Melbourne. Atmospheric winds and their implications for microair vehicles. *AIAA Journal*, 44(11):2591–2600, 2006.

[13] T Weis-Fogh. Quick estimates of flight fitness in hovering animals, including novel mechanisms for lift production. *Journal of Experimental Biology*, 59:169–230, 1973.

[14] J Wu and M Sun. The influence of the wake of a flapping wing on the production of aerodynamic forces. *Acta Mechanica Sinica*, 21:411–418, 2005.

Copyright Statement